Coral Reefs
https://doi.org/10.1007/s00338-025-02727-5

RESEARCH

Skeletal structure and adaptive mechanisms of corals inhabiting a mangrove environment

Dayana Chadda-Harmer[1,2] · Maria Byrne[1,2] · Matthew Foley[3] · Georgia Barrington-Smith[1] · Emma F. Camp[4] · Shawna A. Foo[1,2]

Received: 24 December 2024 / Accepted: 27 July 2025

Abstract Coral skeletons form the foundational framework of coral reef ecosystems but are threatened by climate change stress. Under sub-optimal conditions, skeletal calcification rates decrease, and corals have been observed to form more porous skeletal structures, raising concerns of sublethal effects under future ocean conditions. Understanding how the structure of coral skeletons will be impacted by multiple, co-occurring climate change stressors and how different coral species will respond is of paramount importance to understand the future of coral reefs. Here, we examined the skeletal structure of corals living in a mangrove system. Mangrove environments possess sub-optimal seawater conditions and provide a natural setting to examine the long-term effects of environmental stressors on the skeletons of resident corals as well as identify mechanisms that corals may adopt to survive. Using micro-computed tomography, we investigated the effects of environmental conditions ranging from mangrove habitat to open reef on the skeletal structure of *Pocillopora acuta*, *Acropora* cf. *millepora* and *Montipora* cf. *digitata*, in the northern Great Barrier Reef. Corals were collected from sites with differing distance from the mangrove system at Low Isles. Species-specific structural changes were recorded in coral skeletons in response to distance from the mangroves. *P. acuta* had more porous and thinner skeletons closer to the mangroves, where seawater conditions were sub-optimal. *Montipora* cf. *digitata* was able to maintain a robust skeleton in the mangrove environment. This coral also possessed more dispersed but larger corallites at these sites, potentially availing of increased food availability in mangroves as a mechanism to support skeletal growth. This study suggests the integrity of coral skeletons will be compromised by climate change stress but that some coral species may be able to utilise mechanisms to maintain normal skeletal growth under sub-optimal conditions.

Keywords Coral reef · Climate change · Marginal and extreme environments · Calcification · Micro-computed tomography

Supplementary Information The online version contains supplementary material available at https://doi.org/10.1007/s00338-025-02727-5.

✉ Dayana Chadda-Harmer
dcha5253@uni.sydney.edu.au

[1] School of Life and Environmental Sciences, The University of Sydney, Sydney, NSW 2006, Australia

[2] Marine Invertebrate Futures Group, School of Life and Environmental Sciences, The University of Sydney, Sydney, NSW 2006, Australia

[3] Sydney Microscopy and Microanalysis, The University of Sydney, Sydney, NSW 2006, Australia

[4] Climate Change Cluster, University of Technology Sydney, Sydney, NSW 2007, Australia

Introduction

Coral reefs are critically important marine ecosystems that are rapidly deteriorating under climate change (Hughes et al. 2017; IPCC 2022; Poloczanska et al. 2016). Increasingly warm, acidic, and low oxygen oceanic conditions threaten the survival of scleractinian (hard) corals and their ability to produce robust skeletons (Fantazzini et al. 2015; Hughes et al. 2020; IPCC 2022; Scucchia et al. 2023; Tambutte et al. 2015). Coral skeletons serve as the foundational framework of coral reef ecosystems, providing structurally complex habitats to support marine biomass as well as protecting the coral polyps (Fordyce et al. 2020).

Coral skeletons are formed through calcification, a biologically controlled mineralisation process in which corals

Published online: 18 August 2025

typically produce the calcium carbonate ($CaCO_3$) mineral aragonite and an organic matrix of macromolecules (Allison et al. 2022; Comeau et al. 2022). Carbonate ions required for aragonite biomineralisation are primarily sourced from the ambient seawater surrounding the corals. Key structures of the coral skeleton include the corallite which houses the coral polyp, the calyx (inner area of the corallite in contact with the polyp), the theca (corallite wall), dissepiments (skeletal layers that form beneath the coral polyp as it grows), inter-septal spaces (voids left behind by the growing polyp, primarily in imperforate corals) and channels or canals (primarily in perforate corals) (Dávalos-Dehullu et al. 2008) (Fig. 1).

Climate change stressors reduce the energy corals can allocate to skeletal formation (Al-Horani et al. 2007; Horvath et al. 2016) and decrease the availability of carbonate ions due to ocean acidification (Byrne and Fitzer 2019; Fairhall 1973; Uthicke et al. 2014). Coral skeletons have been observed to become increasingly porous and contain larger inter-septal spaces under climate change conditions, making them more vulnerable to mechanical damage (Fantazzini et al. 2015; Scucchia et al. 2023; Tambutte et al. 2015). This threatens the critical socioeconomic and ecological services that coral skeletons and, by extension, coral reefs provide, such as protecting coasts from destructive waves, supporting commercial and subsistence fishing, as well as providing essential habitat for at least 25% of all known marine species (Fordyce et al. 2020; Hoegh-Guldberg et al. 2019).

As global environmental stressors continue to impinge on the ability of corals to form skeletons, it is imperative to understand how skeletal formation will be impacted by changing water conditions as well as local environmental factors. Coral populations surviving in environments which naturally exhibit sub-optimal conditions provide a long-term setting to examine the effects of stressors on coral skeletons and the adaptive mechanisms corals may adopt to cope in stressful environments (Burt et al. 2020; Camp et al. 2018; Howells et al. 2018; Prada et al. 2021; Schoepf et al. 2023). Mangroves are considered one of the best natural analogues for studying the impacts of projected climate change conditions on corals as the three contemporary climate change stressors (ocean warming, ocean acidification and ocean deoxygenation) can be found to co-occur (Burt et al. 2020; Camp et al. 2019, 2017; Yates et al. 2014). Mangrove environments are characterised by salt tolerant trees and shrubs that colonise intertidal settings. The waters around

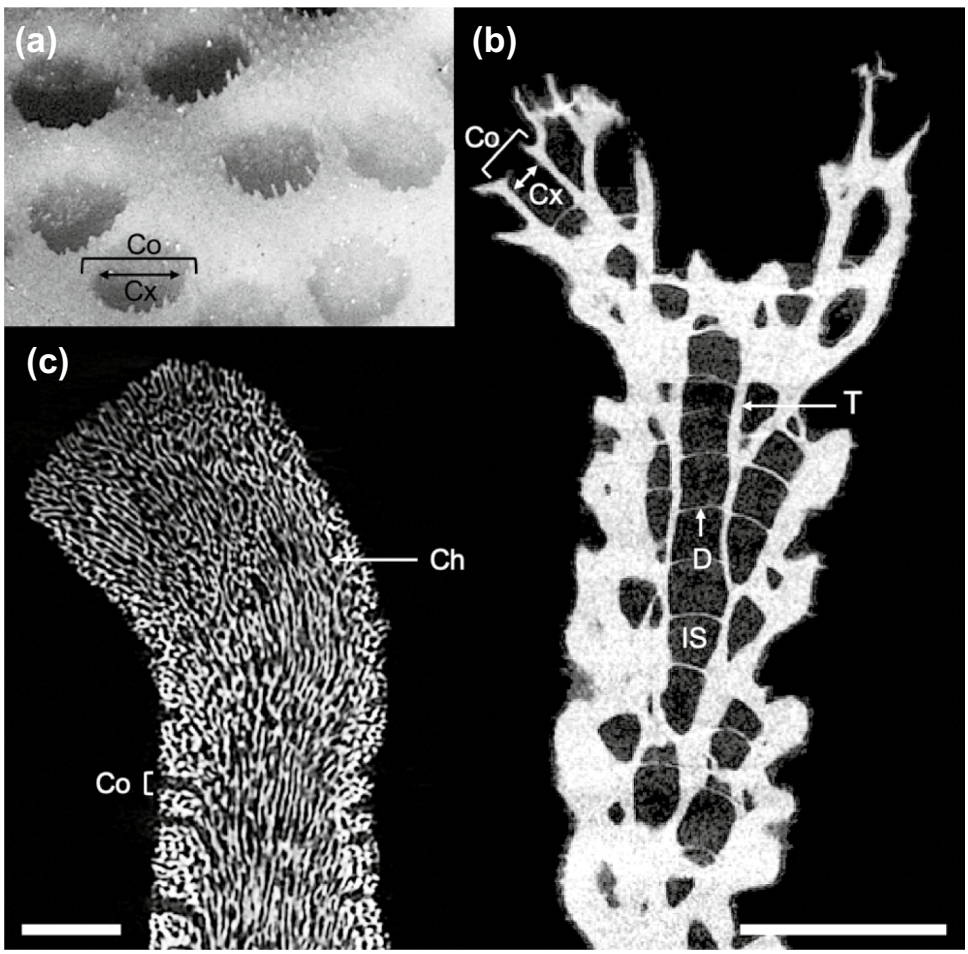

Fig. 1 Coral skeletal structures. **a** Photomicrograph of the surface of a coral skeleton (Co = corallite; Cx = calyx). **b** Micro-computed tomography longitudinal cross section of an imperforate coral (T = theca; D = dissepiment; IS = inter-septal space). **c** Micro-computed tomography longitudinal cross section of a perforate coral (Ch = channel/canal). In imperforate corals, polyp tissues are only connected at the surface of the skeleton while in perforate corals polyp tissues are connected within the skeleton through a network of canals. Scale is 3 mm

mangroves are highly heterogenous and often exhibit low pH, hypoxia and variable temperature whereby mangrove interiors contain the most extreme conditions (Altieri et al. 2019; Camp et al. 2019).

Corals in mangrove environments show 30–40% lower calcification rates compared to those on non-mangrove reefs, indicating reduced skeletal formation under stressful/less optimal conditions (Camp et al. 2016). Although decreased calcification rates have been observed at mangroves, the impact of these environments on the structural features of coral skeletons remains largely unknown. Recent work for one species of coral, *Porites lutea*, suggested reduced skeletal density and higher porosity for mangrove corals compared to adjacent reef corals (Scucchia et al. 2023). However, whether this observation is true for other coral species, and how geographic distance to mangroves impacts skeletal structures remains untested. As skeletal structural integrity is critical for coral survival, examining coral skeletons from mangrove environments provides important insights into how corals may be impacted by near future ocean conditions (Scucchia et al. 2023).

Mangrove associated corals are also recorded to have increased rates of respiration (Burt et al. 2020; Camp et al. 2019, 2017). At Low Isles in the Great Barrier Reef, Camp et al. (2019) recorded a 11–35% increase in mangrove associated coral respiration rates. As corals can gain energy via both photosynthetic dinoflagellate endosymbionts (zooxanthellae) as well as through heterotrophic feeding, enhanced respiration is suggested to indicate an increased reliance on heterotrophic energy which may be a potential mechanism for coral survival under sub-optimal conditions (Burt et al. 2020; Love et al. 2025). Corals possessing larger calyxes or more abundant corallites are suggested to have a greater ability to capture planktonic prey and is another measure used to assess coral dependence on heterotrophy (Conti-Jerpe et al. 2020; Houlbreque and Ferrier-Pages 2009). The high productivity of organic matter from mangroves and abundant zooplankton, is suggested to increase heterotrophic feeding opportunities in mangrove environments (Granek et al. 2009; Perry 2007). However, as trophic preferences vary between corals, the extent of heterotrophy is dependent on the coral species, proximity to mangroves, and currents affecting nutrient delivery (Granek et al. 2009; Houlbreque and Ferrier-Pages 2009).

Here, we present a multi-species assessment of coral skeletal structure in a mangrove environment. Corals from across a mangrove to reef gradient were studied using a combination of micro-computed tomography and photomicroscopy image analysis techniques to assess i) whether environmental conditions as found in mangrove systems impact the structure of coral skeletons and over what distances these effects may occur; and ii) whether corals from mangrove environments exhibit larger calyxes or more numerous corallites indicative of increased heterotrophic feeding as a potential coping mechanism under stress conditions. Three species of branching scleractinian corals were investigated: *Pocillopora acuta*, *Acropora* cf. *millepora* and *Montipora* cf. *digitata.* It was hypothesised that coral skeletons would be less robust (more porous and thinner) closer to the mangroves where conditions are sub-optimal; but that species-specific responses may occur as corals may be able to utilise the available organic matter at mangroves through heterotrophy to compensate for energy loss due to stress.

Methods

Study sites

This study was conducted in the northern Great Barrier Reef, Australia at the mangrove waterways of Woody Island, Low Isles (16º 23' S, 145º 34' E) and adjacent reefs of Low Isles (16º 23' S, 145º 34' E) as well as at Opal Reef (16º 13' S, 145º 53.5' E) which serves as a control (reference) site (Fig. 2). The physiochemical water conditions at Low Isles differ between the mangrove environment and adjacent reef. Amongst the mangroves, the average diel water temperature is 28 ºC and temperature has been recorded to fluctuate up to 7.7 ºC over a diurnal cycle (Camp et al. 2019; Haydon et al. 2021). The adjacent reef experiences more stable conditions with approximately 1 ºC diel fluctuations and an average water temperature of 26 ºC (Haydon et al. 2021). Mangrove waters at Woody Island also have a lower pH and dissolved oxygen content (pH = 7.74–7.81, oxygen = 2.5–4.1 mg/L) compared to the adjacent Low Isles reef (pH = 8.08–8.11, oxygen = 6.2–6.8 mg/L) (Haydon et al. 2021). There is no record of a freshwater source at Low Isles but reductions in salinity are recorded after heavy rains from the influence of river plumes due to the proximity of Low Isles to the Daintree and Mossman rivers (Bartels et al. 2023). Opal Reef is located approximately 38 km north-east of Low Isles and is considered to possess optimal conditions for coral growth without mangrove influence (Chadda-Harmer et al. 2025). Opal Reef experiences average water temperature of 26 ºC, with temperatures ranging from 23 to 29 ºC on average (Howlett et al. 2021). Average pH and oxygen levels at Opal Reef are 8.1 and 6.5–6.9 mg/L respectively (eReefs 2019).

To investigate the influence of proximity to mangrove lagoons on coral skeletal structure, coral and sediment samples were collected from five sites (Fig. 2) at differing proximities to the mangroves: (1) Mangrove Lagoon, (2) Mangrove Channel, (3) Inner Adjacent Reef, (4) Outer Adjacent Reef and (5) Opal Reef. The Mangrove Lagoon and Mangrove Channel sites are located amongst the mangrove plants at Woody Island. The Mangrove Lagoon site is a broad mangrove encapsulated lagoon deep in the interior

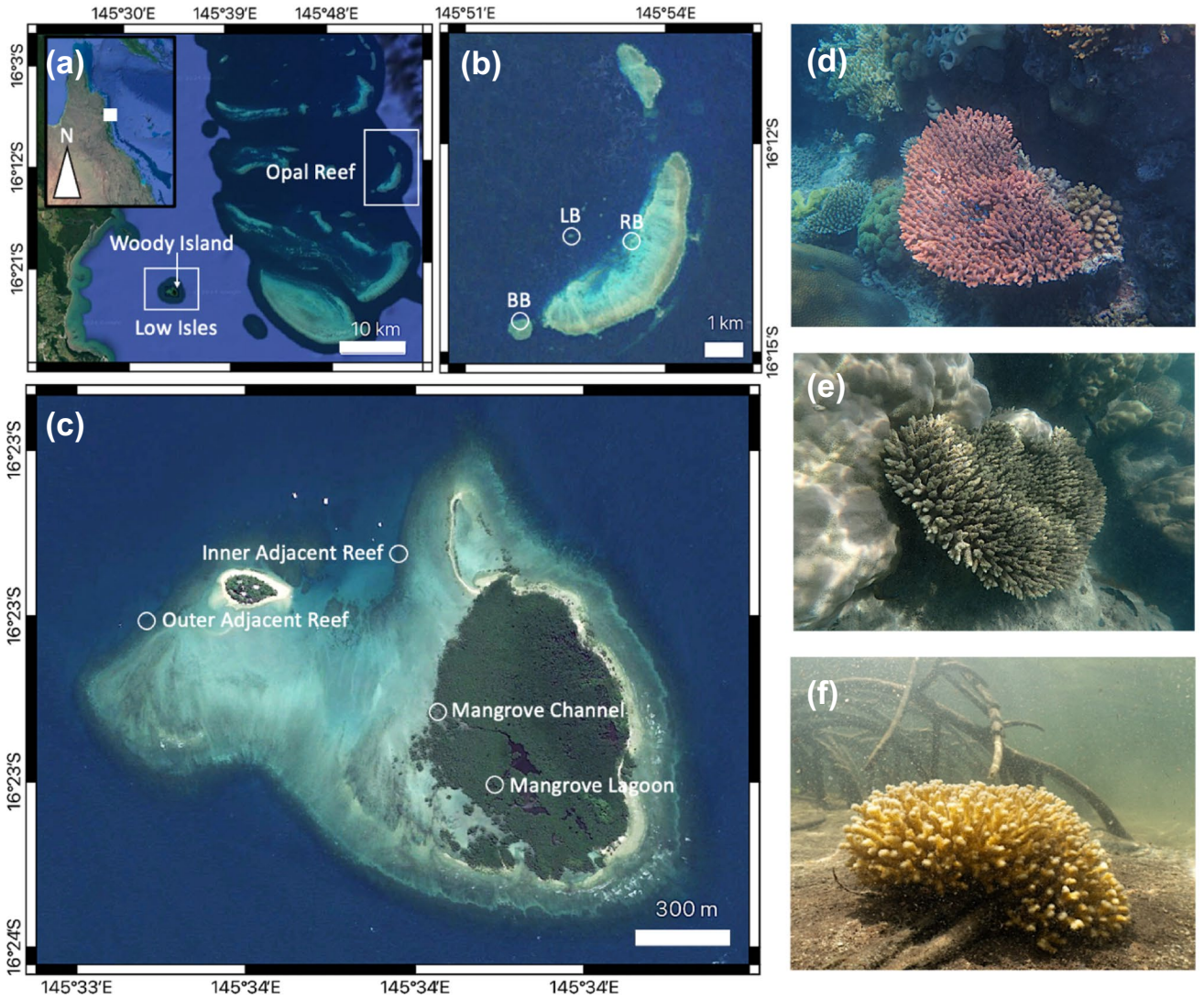

Fig. 2 Map of sampled sites (white circles) in the Great Barrier Reef, Australia (Google Earth). **a** Comparative location of Woody Island, Low Isles and Opal Reef. Inset map shows the study area (white square) in the context of Queensland, Australia. **b** Opal reef with sampling locations at Long Bommie (LB), Rayban (RB) and Bashful Bommie (BB). **c** Low Isles with the Mangrove Lagoon and Mangrove Channel sites at Woody Island and the Inner Adjacent Reef and Outer Adjacent Reef sites at the Low Isles reef. All maps maintain a northward orientation. Coral colonies from **d** Opal Reef, **e** Low Isles reef and **f** amongst the mangroves at Woody Island

of the swampland. The Mangrove Channel site is a narrower mangrove lined channel. Samples were collected from the middle of the waterway so that there was no influence of shading from the mangrove canopy. Only coral colonies growing on the sediment substrate were sampled i.e., not corals growing on mangrove roots. The Inner Adjacent Reef and Outer Adjacent Reef sites are located on the Low Isles reef margin next to the mangroves and are 350 m and 1 km away from the mangroves respectively. Sites were located on the leeward (western) side of the mangroves which has reduced influence from wave action. At the Opal Reef site, samples were collected from three main regions of the reef – Long Bommie, Rayban and Bashful Bommie –located on the protected leeward side of the reef. Samples were collected across the different reef regions to account for natural variation at the control site. These samples were pooled and considered collectively as Opal Reef.

Sample collection and preparation

Coral fragments 1–5 cm in length were collected by hand (using side cutters) from the apical branches of coral colonies at water depths less than 2.5 m at the Woody Island mangroves, Low Isles reef and Opal Reef in October 2022. There had been no significant rainfall in the time leading up to sampling. Three species of branching coral were sampled:

Acropora cf. *millepora, Montipora* cf. *digitata, and Pocillopora acuta*. The number of samples collected was determined by the number of colonies available for each species at each site, where not all species were present at each site (Table 1). One sample of the surficial sediment substrate directly surrounding corals was also collected at each site. Skeletons were prepared for analysis by submerging coral fragments in a 10% sodium hypochlorite solution for 24 h to remove coral tissue. Samples were then rinsed with distilled water and dried at room temperature for 48 h.

Micro-computed tomography

To examine the skeletal structure, coral fragments were scanned using a Bruker SkyScan 2214 micro-computed tomography (micro-CT) system at the University of Sydney Microscopy and Microanalysis Research Facility, Sydney, Australia (Fig. 3a). This micro-CT system uses a tungsten filament cathode source to generate x-rays, which are transmitted through the sample and collected by a suitable detector. Entire samples were scanned individually and secured to the rotating stage using dental wax to minimise sample movement and improve image quality. Multiple projections were collected at regular angular intervals as the sample was rotated. A flat field correction was run at the start of each scanning set to calibrate the detector and ensure consistency amongst scans. Samples were scanned in a randomised order to avoid any potential confounding effects of source power variation (Decarlo 2017). To generate the best image quality regardless of the size, thickness and structural complexity of samples, settings for scanning and reconstruction varied between imperforate (*P. acuta*) and perforate (*A.* cf. *millepora* and *M.* cf. *digitata*) species (Fig. 3b, Table 2).

X-ray attenuation data from multiple two-dimensional (2D) scans were reconstructed using Nrecon software (version 2.2.0.6) to form a series of cross-sections representing a three-dimensional (3D) object. Ring artefact reduction and beam hardening (Supplementary Material: S.1) correction values were specified in Nrecon (Table 2) and a mathematical misalignment compensation factor was also specified for each scan to correct for any misalignment in the rotational stage axis relative to the detector (centre shift). Reconstructed scans were rendered as 3D models using the Bruker micro-CT volume rendering software CTvox (version 3.3.0.0) and the inspection software Dataviewer (version 1.6.0.0) was used to generate 2D longitudinal and transverse cross-sections. The integrity of each coral sample was checked within CTvox by visually examining for any signs of disease or microborers. The top 1 cm of coral fragments was manually defined for data extraction within CTAn by measuring 1 cm downwards from the top of coral fragments oriented in the direction of growth (Fig. 3c). This controlled for variations in the size of fragments and allowed analysis to consistently assess the most recent growth which was important to consider as previous studies have reported changes in structural features (such as a reduction in porosity) across the length of coral samples due to factors such as the active infilling of pores with growth over time (Caroselli et al. 2011; Chamberlain 1978; Gladfeiter 1982; Roche et al. 2011). It was noted that more tip material was added in four samples which had branches at differing heights (i.e., not on the same transversal plane) (Fig. 3c).

Quantitative data from micro-CT reconstructions were extracted using the Batch Manager function within the Bruker CT-Analyser (CTAn) software (version 1.18.8.0). Otsu's thresholding method (Otsu 1979) was used within CTAn to differentiate between the sample material and air within a scan using differences in grey scale intensity, representing variations in the x-ray beam attenuation as a result of sample composition. The shrink-wrap algorithm within CTAn was used to define the region of analysis to the edge of each threshold object so that there was no non-sample space analysed. Data were extracted for two quantitative parameters: (1) object surface to volume ratio and (2) structure thickness. (1) Object surface to volume ratio (surface area to volume ratio) is a measure of the solid surface area of the skeletal sample divided by the sample volume. This ratio is calculated by interpolating 2D scans to find an

Table 1 Summary of site locations and the number of coral samples collected

Site	GPS Location	Depth (m)	Coral Samples		
			Pocillopora acuta	*Montipora* cf. *digitata*	*Acropora* cf. *millepora*
Mangrove Lagoon	16°23′25'' S, 145°34′00''E	0.47	6	0	0
Mangrove Channel	16°23′16'' S, 145°33′55''E	0.39	6	6	0
Inner Adjacent Reef	16°23′00'' S, 145°33′51''E	0.48	7	5	6
Outer Adjacent Reef	16°23′08'' S, 145°33′24''E	0.62	7	0	7
Opal Reef (LB)	16°13′24'' S, 145°52′37''E	2	4	0	0
Opal Reef (RB)	16°13′22'' S, 145°53′26''E	2.4	0	0	7
Opal Reef (BB)	16°14′32'' S, 145°51′50''E	2.1	2	0	0

LB = Long Bommie, RB = Rayban, BB = Bashful Bommie.

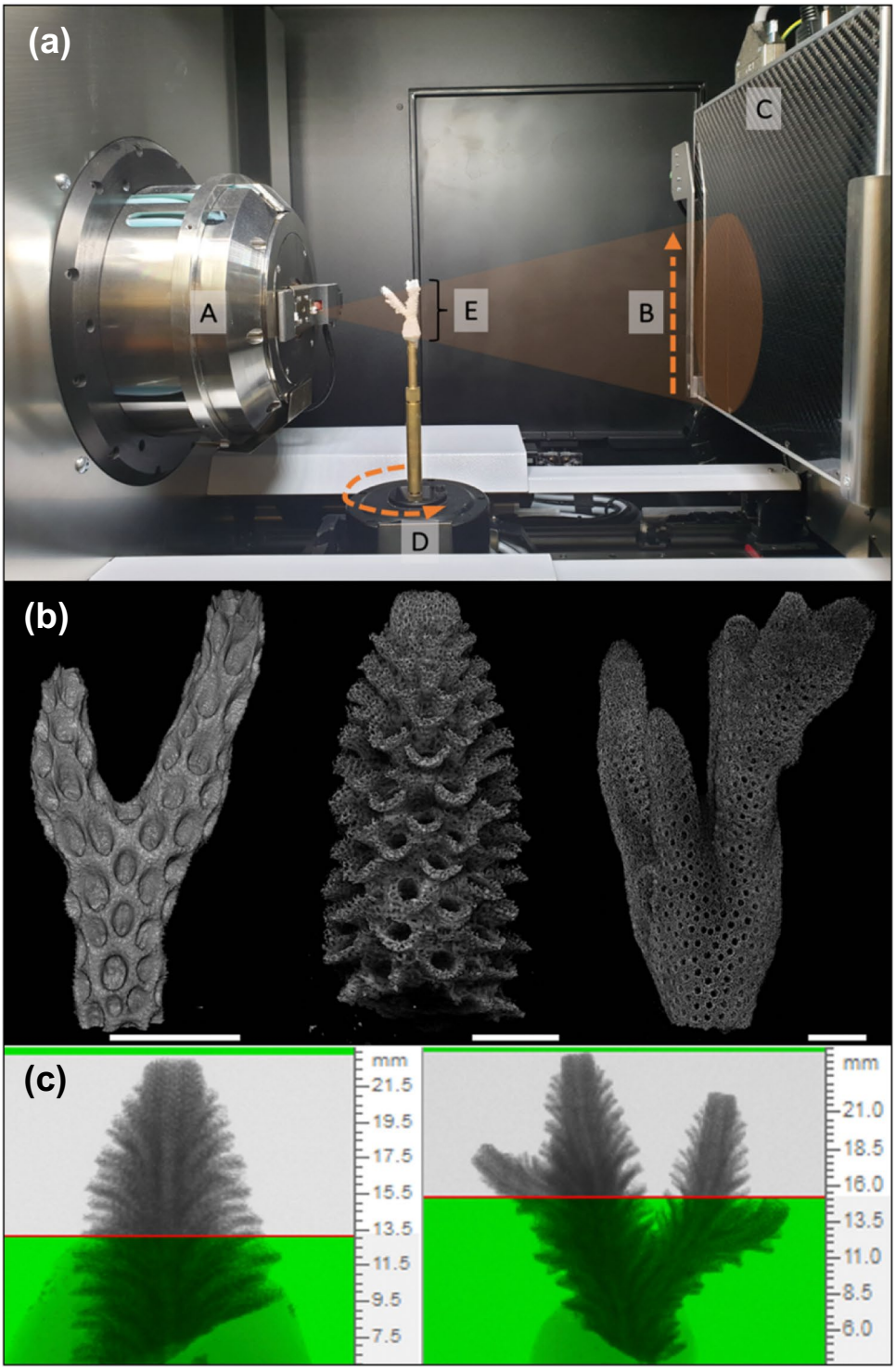

Fig. 3 **a** Micro-computed tomography setup within the Bruker SkyScan 2214 system. (A) X-ray source, (B) x-ray transmission which passes through the sample and reaches the detector. For taller samples, multiple scans were collected at specific vertical positions and stitched together during reconstruction, (C) flat panel detector, (D) rotating stage, (E) coral sample secured to a stand with dental wax. **b** Representative samples of coral species investigated (left to right): *Pocillopora acuta*, *Acropora* cf. *millepora* and *Montipora* cf. *digitata*. Micro-computed tomography images generated using CTVox (SkyScan, Bruker 3D Suite). Scales = 5 mm. **c** Defining the top 1 cm region of coral samples used for analysis in the CT-Analyser software. Grey zones in the image mark the top 1 cm region. Measurements were taken from corals oriented in the direction of growth (left-hand panel) but four samples with multiple branches led to additional 'top' material being analysed (right-hand panel)

average surface to volume ratio for each sample. The surface to volume ratio parameter characterises the complexity of structures and can be used to infer skeletal porosity (Supplementary Material: S.2). More pores increase the sample surface area and reduce the sample volume. Consequently, a higher surface area to volume ratio indicates a more porous and structurally complex skeleton. A limitation of this parameter as a measure of porosity, however, is that it may also be influenced by protruding corallite structures which, if present, can contribute to a higher surface to volume ratio being recorded. (2) Structure thickness (thickness) measures the 3D thickness of skeletal features and, as a single sample is made up of skeletal structures of varying thicknesses,

Table 2 Settings used for Micro-Computed Tomography Scanning and Reconstruction

Micro-CT Component	Setting	Coral Species		
		Pocillopora acuta	*Montipora* cf. *digitata*	*Acropora* cf. *millepora*
X-ray source	Voltage (kV)	120	60	60
	Current (µA)	80	200	200
X-ray detection	Filter	Aluminium Copper (Al 1 mm + Cu 0.075 mm)	Absent	Absent
Image capture	Sample rotation (°)	360	180	180
	Image collection interval (°)	0.4	0.2	0.2
	Resolution (µm)	12	15 – 25	15 – 25
	Exposure (ms)	1831	250	250
Reconstruction	Beam hardening correction (%)	50	60	60
	Ring artefact correction	7	7	7

To maintain an equivalent quality of imaging between samples, one sample of *A.* cf. *millepora* was analysed using x-rays generated from a source operating at 90 kV voltage and 100 µA current due to its greater size and thickness. Because of the higher voltage used, an aluminium filter (Al 1 mm) was applied to avoid beam hardening and consequently the beam hardening correction was lowered to 45% for that sample.

the distribution of thicknesses within each sample can be calculated.

Corallite morphometrics

To determine calyx size and corallite density, the surface of coral fragments was examined under an Olympus stereo microscope (model SZX10) and photographed using the Olympus cellSens Standard 3.2 imaging software. Three or more images were collected from each fragment focusing on the top 3 cm on the skeleton and ensuring images were representative of the entire surface. Corallite measurements were taken from photomicrographs using the image processing software ImageJ (version 2.9.0) (Schneider et al. 2012). The diameter of 10 representative calyxes were measured from each coral fragment. Only calyxes 5–30 mm below the branch tip were selected to avoid new calyxes at variable stages of growth and to ensure consistency across samples. Where available, calyxes from multiple branches were measured. Diameters were measured perpendicular to the growth axis using the straight line tool as per Kramer et al. (2022) (Fig. 4a). To determine the density of corallites, the polygon selection tool was used to measure the surface area of a region of skeleton and the number of corallites within that region were counted. Surface area measures were focused on the centre of branches to avoid any curvature of the skeleton that may have obscured the presence of corallites; the largest available surface area which met these criteria was used

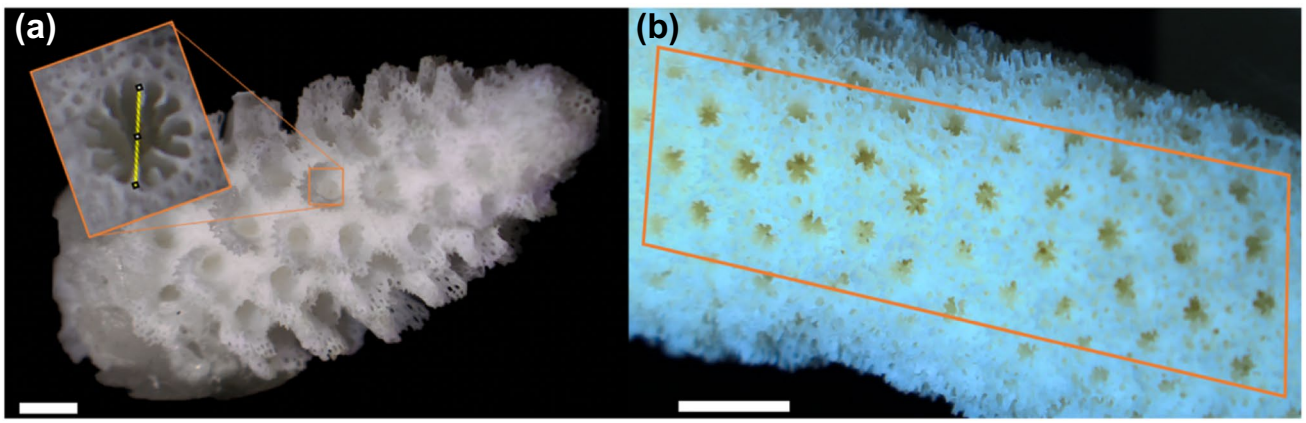

Fig. 4 Collection of corallite morphometrics using photomicrographs in ImageJ. **a** Measurement of calyx diameter perpendicular to the axis of growth from corallites within a band 5–30 mm below the growth tip (inset image not to scale). **b** Measuring the surface area of a region of skeleton. Scales = 1 mm

(Fig. 4b). Whole and partial corallites that were at least half within the surface area region were measured. The density was calculated by dividing the number of corallites by the surface area. Measurements were conducted in a randomised order across samples.

Statistical analysis

To examine the impact of mangrove association on coral skeletal structure, data were statistically analysed using R software version 4.2.2 (R Core Team 2022). For all parametric analysis, model assumptions were assessed by inspecting plots of residuals vs. fitted values for homogeneity of variance as well as Q-Q plots and histograms for normality. The 'ggplot2' package version 3.4.1 (Wickham 2016) as well as the 'performance' package version 0.13.0 (Lüdecke et al. 2021) were used to evaluate model assumptions. The 'tidyverse' package version 2.0.0 (Wickham et al. 2019) in R was used for data wrangling. Data visualisation was made in R using the 'ggplot2' package (Wickham 2016). Statistical significance was set at $p < 0.05$.

A linear model was used to compare the surface area to volume ratio of coral skeletons across sites and species. Surface area to volume ratio was the response variable while site and species were fixed factors with five and three levels respectively. Data were logarithmically transformed to meet assumptions and outputs derived using the 'summary' and 'anova' functions in R. Results found to be significant were analysed using a pairwise post-hoc comparison via the 'emmeans' package with p value adjustment set to the Tukey method (Lenth 2025).

Structural thickness distributions for each sample were compiled by species and site and converted to frequencies using the 'rep' function in R. Skeletal thickness across sites were then visualised separately for each species using kernel density estimate plots. The density plot function in R uses a Gaussian kernel density estimator and the Silverman's rule of thumb (Silverman 1986) bandwidth function to define the smoothness of plots. This default function works best with normal data and the plots of species containing non-normal data (*A.* cf. *millepora, M.* cf. *digitata*) were found to be undersmoothed. The bandwidth for these plots was adjusted iteratively and set at 0.03. As structural thickness distribution data showed the frequency of skeletal material across discrete thickness classes, Kolmogorov–Smirnov two-sample tests were used to compare thickness-frequency distributions between sites for each species. This non-parametric approach was chosen due to the lack of normality in the data.

Differences in the calyx diameter across sites and species were tested for using a linear mixed-effects model constructed from the 'lme4' package (Bates et al. 2015) with site and species as fixed factors and sample nested within site as a random factor. Corallite density data were square root transformed to meet assumptions and analysed using a linear model to examine the effect of site and species, specified as fixed factors. Outputs for calyx diameter and corallite density were derived using the 'summary' and 'anova' functions in R. For the calyx diameter, a Type III analysis of variance using Satterthwaite's method was conducted within the 'lmerTest' package version 3.1.3 (Kuznetsova et al. 2017). Results found to be significant were analysed using a pairwise post-hoc comparison via the 'emmeans' package with p value adjustment set to the Tukey method (Lenth 2025).

Organic matter content

To characterise the organic matter content at each site, sediment samples were analysed using the loss on ignition method (Dean 1974; Heiri et al. 2001). Sediments were first dried in a Binder drying chamber for three days at 50 ºC. Two 20–25 g subsamples were then taken from each dried sediment sample (subsamples, n = 12) and placed in ceramic crucibles. Subsamples were divided using a riffle splitter to homogenise sediments. Crucibles containing sediments were placed in a Labec muffle furnace and heated to 550 ºC for four hours. Sediments were removed once the furnace had cooled to 96 ºC. Samples were weighed using a digital balance (Mettler Toledo AE160) both before ($weight_{initial}$) and after ($weight_{550}$) being heated in the furnace. Any weight loss observed was assumed to correspond to the amount of organic matter present, as organic carbon combusts at temperatures between 500 and 550 ºC (Heiri et al. 2001). The percentage of organic matter in each subsample was calculated using Eq. (1). The two subsamples served as a procedural control and as similar results were obtained from each, the results were averaged to determine a single percentage of organic matter content for each sample.

$$Organic\ matter\ (\%) = \frac{\left(weight_{initial} - weight_{550}\right)}{weight_{initial}} \times 100 \quad (1)$$

Results

Surface area to volume ratio

Analysis of the surface area to volume ratio of coral skeletons revealed differences between species ($F_{2,51} = 53.980$, $p < 0.001$) and across sites ($F_{4,51} = 2.754$, $p = 0.038$) as well as an interaction between species and site ($F_{3,51} = 3.758$, $p = 0.016$; Fig. 5). The surface area to volume ratio of *P. acuta* differed from both *M.* cf. *digitata* ($p < 0.001$) and *A.*

cf. *millepora* ($p < 0.001$). However, there was no difference between *M.* cf. *digitata* and *A.* cf. *millepora* ($p = 0.993$).

Post hoc analysis showed that in *P. acuta*, the surface area to volume ratio at both the Mangrove Lagoon and Mangrove Channel sites differed significantly from the Inner Adjacent Reef, Outer Adjacent Reef and Opal Reef sites (Table S1, Fig. 6a). However, there was no significant difference amongst the sites within the mangroves or amongst the sites outside of the mangroves (Table S1; Fig. 6a). The highest surface area to volume ratios were recorded at the Mangrove Lagoon and Mangrove Channel sites (Fig. 6a). These findings support visual assessment of micro-CT cross-sections which showed fragments from the Mangrove Lagoon and Mangrove Channel sites were porous and contained large chambers i.e., inter-septal spaces separated by thin corallite walls and thin dissepiments across the length of the coral fragments; whereas the skeletons from other sites contained smaller inter-septal spaces and were less porous, particularly around the edge of the fragments (Fig. 6e). The structure of skeletons appeared similar at the Inner Adjacent Reef, Outer Adjacent Reef and Opal Reef sites despite being from differing distances to the mangroves (Fig. 6e).

Specimens of *M.* cf. *digitata* were found at two sites, the Mangrove Channel and Inner Adjacent Reef. There was no difference in the surface area to volume ratio of skeletons from these sites ($p = 0.814$; Fig. 7a). Micro-computed tomography cross-sections also showed that the structure of *M.* cf. *digitata* skeletons were similar at both sites (Fig. 7e). The skeletal structure was highly porous and dominated by spongy coenosteum skeletal material (Fig. 7e).

Specimens of *A.* cf. *millepora* were only found at sites outside of the mangroves—the Inner Adjacent Reef, Outer Adjacent Reef and Opal Reef. Differences in the surface area to volume ratio were recorded between the Outer Adjacent Reef and Opal Reef sites ($p = 0.006$) but no significant differences occurred between the other sites (Table S2). The surface area to volume ratio of *A.* cf. *millepora* skeletons was highest at the Outer Adjacent Reef and lowest at Opal Reef, as seen in micro-CT cross sections (Fig. 8a, e). All *A.* cf. *millepora* skeletons contained a distinct axial canal surrounded by perforate skeleton material (Fig. 8e).

Structural thickness

Kolmogorov–Smirnov tests showed *P. acuta* skeleton thickness-frequency distributions differed across sites, where both the Mangrove Lagoon and Mangrove Channel sites differed from the Inner Adjacent Reef, Outer Adjacent Reef and Opal Reef sites ($p < 0.000$; Table S1) and the Inner Adjacent Reef and Opal Reef also differed ($D = 0.108$, $p = 0.007$). Density plots showed that the distribution of skeleton thickness from mangrove sites was strongly right skewed and leptokurtic. Corals from the Mangrove Lagoon and Mangrove Channel sites had a higher proportion of thinner skeletal structures (mean thickness ± standard error (SE), 0.386 ± 0.009 mm (n = 6) and 0.372 ± 0.007 mm (n = 6), respectively) (Fig. 6b). In comparison, corals from the Inner Adjacent Reef, Outer Adjacent Reef and Opal Reef sites contained thicker skeletal structures (mean thickness ± SE of 0.876 ± 0.019 mm (n = 7), 0.810 ± 0.017 mm (n = 7), and 0.771 ± 0.019 mm (n = 6),

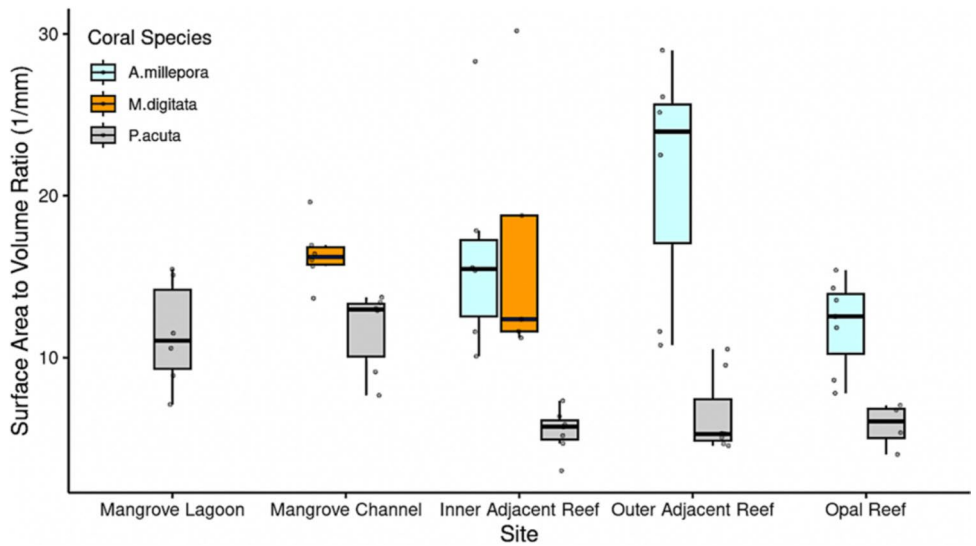

Fig. 5 Inter-species comparison of skeletal surface area to volume ratio of corals from sites at varying distances to a mangrove system. The Mangrove Lagoon and Mangrove Channel sites are amongst the mangroves, the Inner Adjacent Reef site is 350 m away from mangroves, the Outer Adjacent Reef is 1 km from mangroves and Opal Reef is 38 km from mangroves. Coral species are *Pocillopora acuta*, *Montipora* cf. *digitata* and *Acropora* cf. *millepora*. In the figure, the box indicates the interquartile range, the horizontal line marks the median, whiskers show the minimum and maximum value within 1.5 × the interquartile range. Dots represent raw values

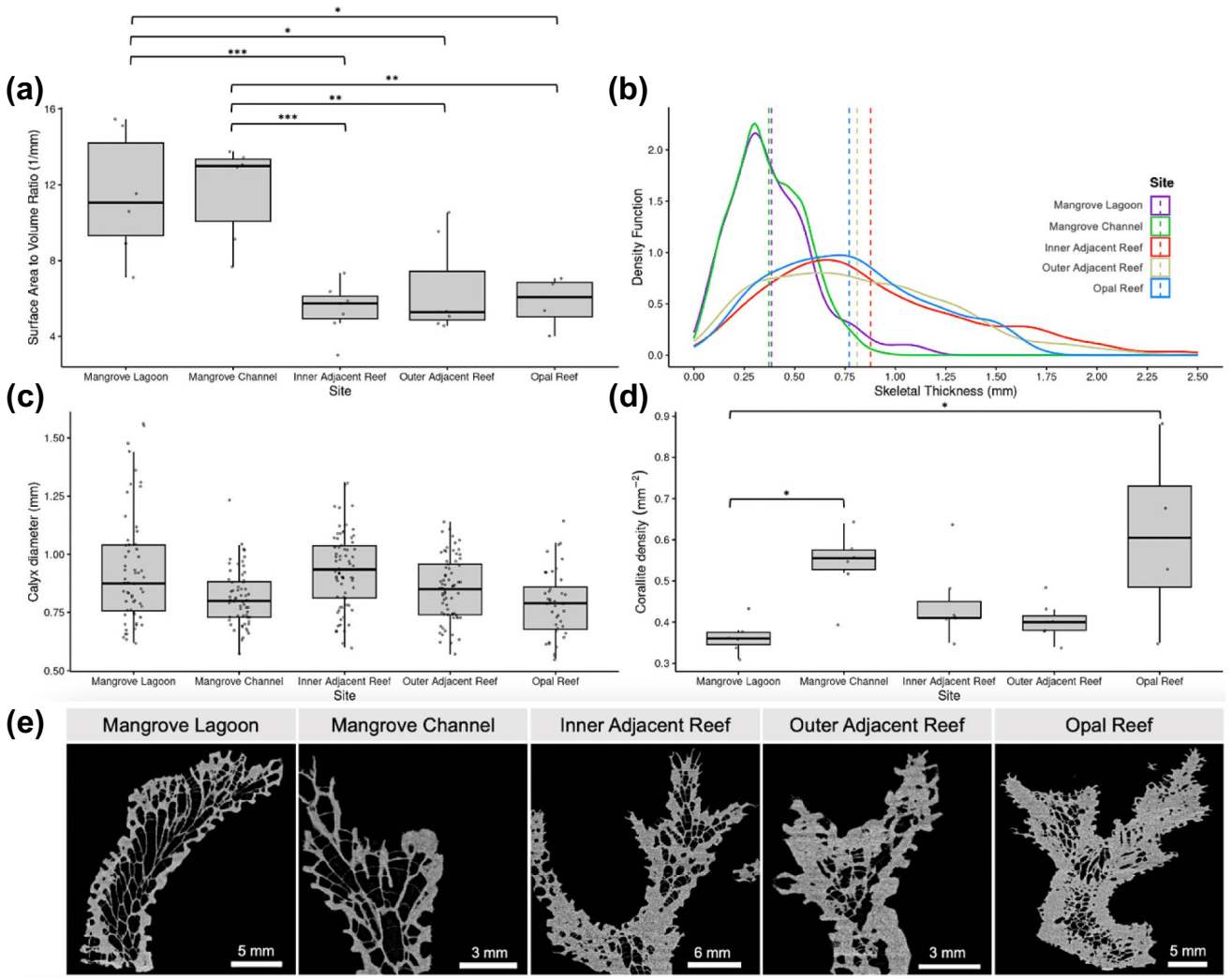

Fig. 6 Skeletal features of *Pocillopora acuta* from sites at varying distances to a mangrove system. The Mangrove Lagoon and Mangrove Channel sites are amongst the mangroves, the Inner Adjacent Reef site is 350 m away from mangroves, the Outer Adjacent Reef is 1 km from mangroves and Opal Reef is 38 km from mangroves. **a** Skeletal surface area to volume ratio (n = 6 for Mangrove Lagoon, Mangrove Channel and Opal Reef sites; n = 7 for the Inner Adjacent Reef and Outer Adjacent Reef sites). **b** Thickness frequencies of skeletal structures. Frequencies are expressed as kernel density distributions. Dashed lines mark the mean thickness of skeletal structures from each site. **c** Diameter of calyxes (n = 60 for Mangrove Lagoon, Mangrove Channel and Opal Reef sites; n = 70 for the Inner Adjacent Reef and Outer Adjacent Reef sites). **d** Density of corallites (n = 6 for Mangrove Lagoon, Mangrove Channel and Opal Reef sites; n = 7 for the Inner Adjacent Reef and Outer Adjacent Reef sites). In the figures, the box indicates the interquartile range, the horizontal line marks the median, whiskers show the minimum and maximum value within 1.5 × the interquartile range and dots represent raw values. Asterisks indicate significant differences as computed by pairwise contrasts, *** $p < 0.001$, ** $p < 0.01$, * $p < 0.05$. **e** Micro-computed tomography, representative longitudinal cross sections of the skeleton of *P. acuta* from sites at varying distances from the Low Isles mangrove system

respectively) and had mildly right skewed mesokurtic distributions (Fig. 6b). Cross-sections showed that skeletons from the Inner Adjacent Reef, Outer Adjacent Reef and Opal Reef sites had thicker corallite walls and dissepiments (Fig. 6e).

The thickness-frequency distributions of skeletal structures in *M.* cf. *digitata* samples differed between the Mangrove Channel and Inner Adjacent Reef sites ($D = 0.136$, $p < 0.000$; Fig. 7b). Density plots showed the distributions from both sites were right-skewed and that mean skeleton thicknesses were relatively similar but lower at the Mangrove Channel (mean ± SE, 0.215 ± 0.003 mm) than at the Inner Adjacent Reef site (mean ± SE, 0.226 ± 0.006 mm).

The thickness-frequency distributions of skeletal structures in *A.* cf. *millepora* samples differed between all sites

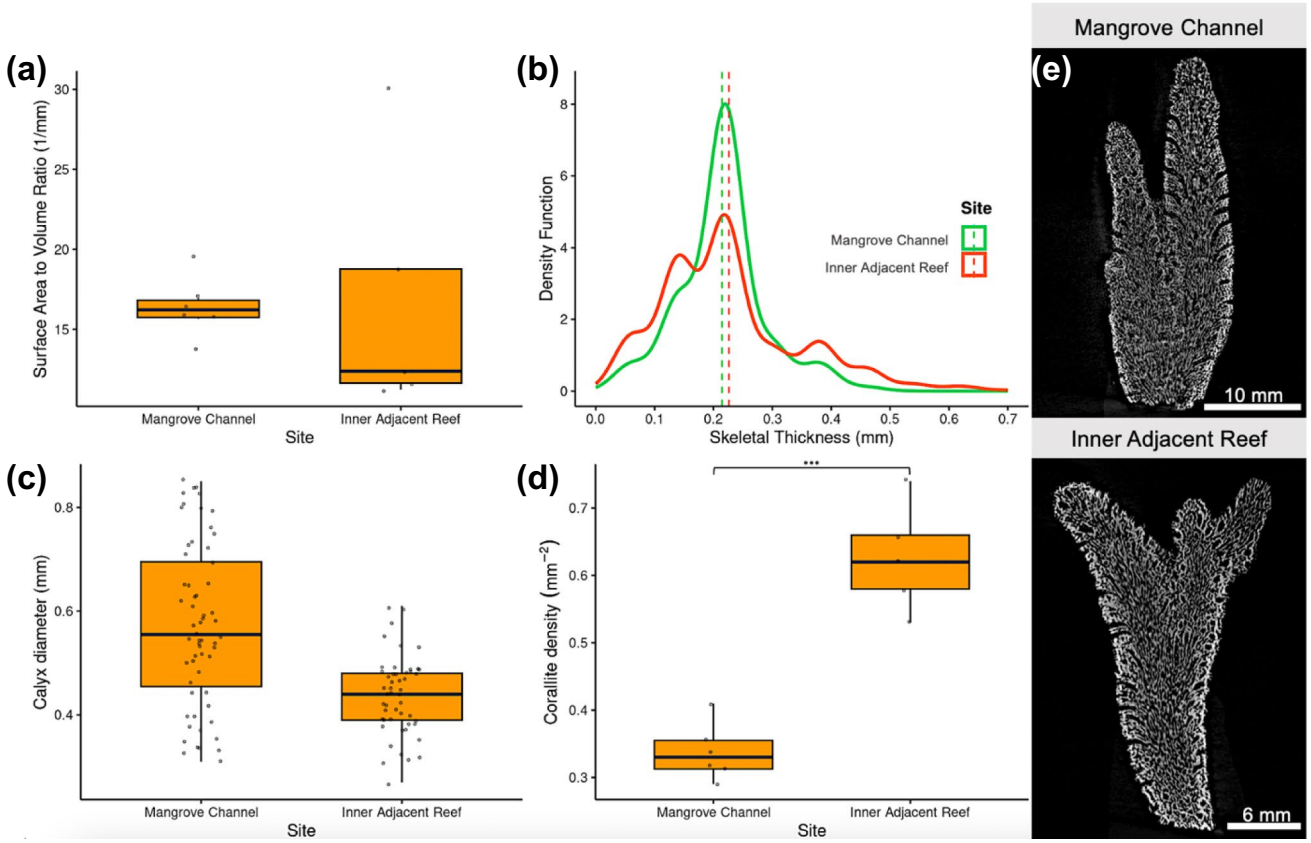

Fig. 7 Skeletal features of *Montipora* cf. *digitata* from sites at varying distances to a mangrove system. The Mangrove Channel site is amongst the mangroves, the Inner Adjacent Reef site is 350 m away from mangroves. **a** Surface area to volume ratio (n = 6 for Mangrove Channel site and n = 5 for Inner Adjacent Reef site). **b** Thickness frequencies of skeletal structures. Frequencies are expressed as kernel density distributions. Dashed lines mark the mean thickness of skeletal structures from each site. **c** Diameter of calyxes (n = 60 for Mangrove Channel site and n = 50 for Inner Adjacent Reef site). **d** Density of corallites (n = 6 for Mangrove Channel site and n = 5 for Inner Adjacent Reef site). In the figures, the box indicates the interquartile range, the horizontal line marks the median, whiskers show the minimum and maximum value within 1.5 × the interquartile range and dots represent raw values. Asterisks indicate significant differences as computed by pairwise contrasts, *** $p < 0.001$. **e** Micro-computed tomography, representative longitudinal cross sections showing *M.* cf. *digitata* skeleton morphology from sites at varying distances to a mangrove system

($p < 0.000$; Table S2). Coral skeletons from the Outer Adjacent Reef had a higher proportion of thin skeletal structures (mean thickness ± SE, 0.198 ± 0.005 mm) in comparison to samples from the Inner Adjacent Reef and Opal Reef sites (mean thickness ± SE, 0.235 ± 0.005 mm and 0.326 ± 0.007 mm, respectively) (Fig. 8b). Corals from Opal Reef possessed the thickest skeletal structures and density plots showed all distributions were right skewed (Fig. 8b). Micro-computed tomography cross sections also showed that specimens from Opal Reef had the thickest skeletal structures, whereas those from the Outer Adjacent Reef had the finest structures, while skeletal features of corals at the Inner Adjacent Reef site appeared to be an intermediate between those observed at the other two sites (Fig. 8e).

Calyx size

Calyx diameter was found to differ between species ($F_{2,51} = 27.334$, $p < 0.001$; Figs. 6, 7 and 8c) but not across sites ($F_{4,51} = 0.840$, $p = 0.506$) and there was no interaction between species and site ($F_{3,51} = 2.258$, $p = 0.093$). *M.* cf. *digitata* differed from both *P. acuta* ($p < 0.001$) and *A.* cf. *millepora* ($p < 0.001$).

Corallite density

The number of corallites per mm^2 (density) differed between species ($F_{2,51} = 12.213$, $p < 0.001$) but not across sites ($F_{4,51} = 1.504$, $p = 0.213$); there was however an interaction between species and site ($F_{3,51} = 10.062$, $p < 0.001$). The

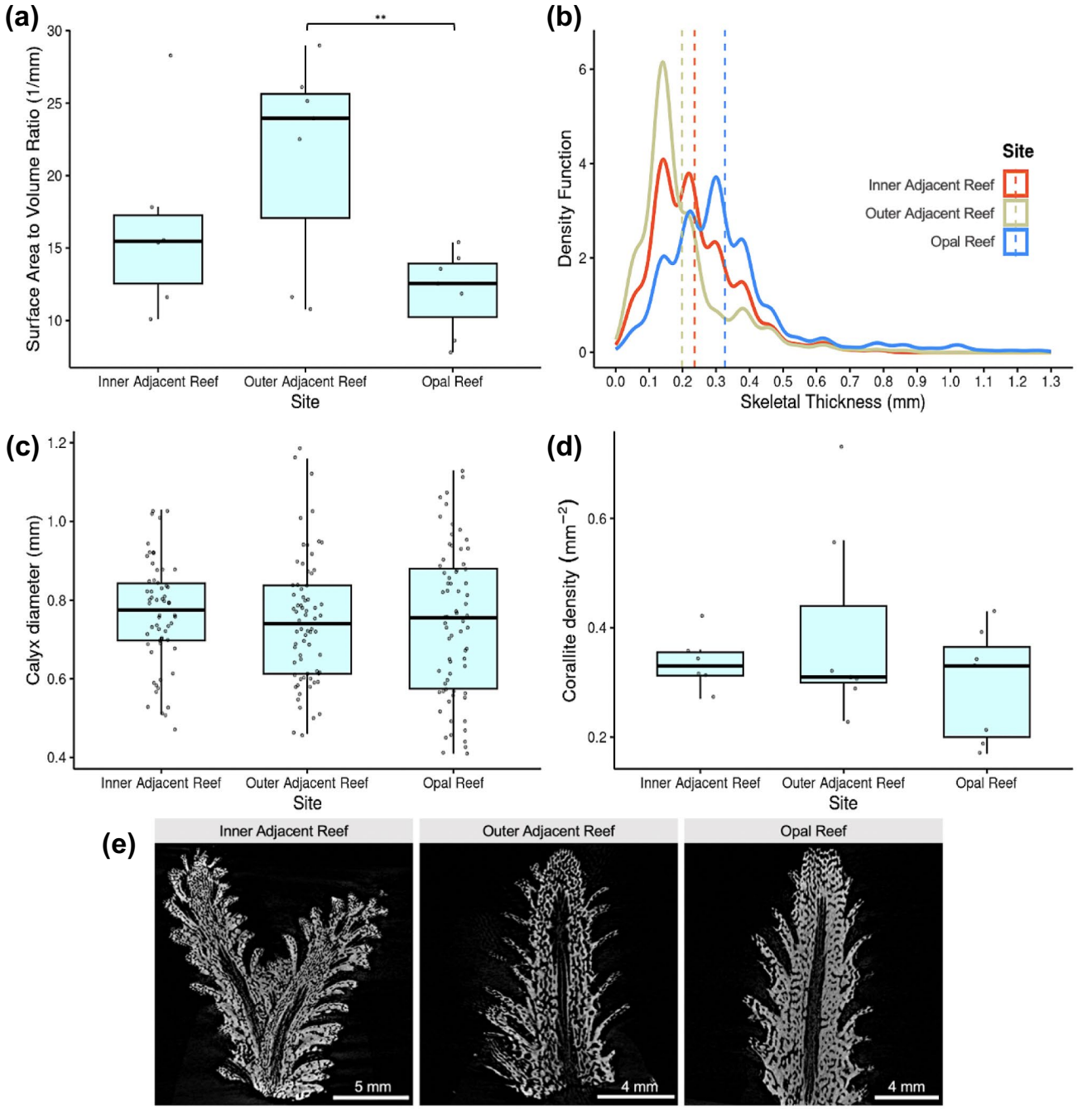

Fig. 8 Skeletal features of *Acropora* cf. *millepora* from sites at varying distances to a mangrove system. The Inner Adjacent Reef site is 350 m away from mangroves, the Outer Adjacent Reef is 1 km from mangroves and Opal Reef is 38 km from mangroves. **a** Surface area to volume ratio (n = 6 for Inner Adjacent Reef site and n = 7 for Outer Adjacent Reef and Opal Reef). **b** Thickness frequencies of skeletal structures. Frequencies are expressed as kernel density distributions. Dashed lines mark the mean thickness of skeletal structures from each site. **c** Diameter of calyxes (n = 60 for Inner Adjacent Reef and n = 70 for Outer Adjacent Reef and Opal Reef). **d** Density of corallites (n = 6 for Inner Adjacent Reef and n = 7 for Outer Adjacent Reef and Opal Reef). In the figure, the box indicates the interquartile range, the horizontal line marks the median, whiskers show the minimum and maximum value within 1.5 × the interquartile range and dots represent raw values. Asterisks indicate significant differences as computed by pairwise contrasts, ** $p < 0.01$. **e** Micro-computed tomography, representative longitudinal cross sections showing *A.* cf. *millepora* skeleton morphology from sites at varying distances to a mangrove system

corallite density of *P. acuta* differed from both *M.* cf. *digitata* ($p = 0.009$) and *A.* cf. *millepora* ($p < 0.001$); and there was a difference between *M.* cf. *digitata* and *A.* cf. *millepora* ($p < 0.001$). Post hoc analysis showed that in *P. acuta*, corallite density differed between the Mangrove Lagoon and Opal Reef sites ($p = 0.016$) as well as the Mangrove Lagoon and Mangrove Channel sites ($p = 0.048$) (Fig. 6d; Table S1). In *M.* cf. *digitata*, differences occurred between the Mangrove Channel and Inner Adjacent Reef sites ($p < 0.001$; Fig. 7d). No differences in corallite density were recorded from *A.* cf. *millepora* (Fig. 8d; Table S2).

Organic matter

The organic matter content detected in sediment samples ranged from 4.39 to 5.11% and was relatively similar across sites. The highest percentage of organic matter was found amongst the mangroves at the Mangrove Channel ($5.11\% \pm 0.14$) and Mangrove Lagoon ($4.91\% \pm 0.11$) sites. At Low Isles, the organic matter content gradually decreases with increasing distance from the Woody Island mangroves (Inner Adjacent Reef site, $4.67\% \pm 0.04$; Outer Adjacent Reef site, $4.39\% \pm 0.06$). However, this trend did not extend to Opal Reef where the percentage of organic matter fell within the range found at Low Isles (Opal Reef: Bashful Bommie, $4.66\% \pm 0.24$; Rayban, $4.52\% \pm 0.01$).

Discussion

We observed species-specific changes in the structure of coral skeletons in response to the environmental stress gradient produced by the Low Isles mangrove system. For *P. acuta*, corals found in the mangroves had significantly more porous and thinner skeletons than corals from the adjacent or control reef. These findings support the hypothesis that coral skeletons are less robust in mangrove environments. The encrusting coral *Porites lutea* was also recorded to possess a more porous skeleton at the Low Isles mangrove system (Scucchia et al. 2023). As mangrove environments contain multiple co-occurring stressors such as low pH, high and variable temperatures as well as low oxygen conditions (Camp et al. 2019), it is suggested that these conditions impinge on the ability of corals to produce robust skeletons (Camp et al. 2017; Tanvet et al. 2022).

It has been suggested that the formation of a more porous and thinner skeleton under sub-optimal conditions is a fitness trade-off strategy which occurs in response to a loss of energy and/or carbonate ions required for skeletal formation as corals prioritise maintaining normal rates of linear extension as opposed to infilling pores to ensure access to light or reach a critical size for sexual maturity (Fantazzini et al. 2015; Scucchia et al. 2023; Tambutte et al. 2015). We suggest another possible explanation for the observed increased porosity under stress conditions may be the result of an imbalance in calcification stages (Neder et al. 2022; Wooldridge 2013). Dark-calcification produces a porous skeletal framework and leads to linear extension (Barnes and Crossland 1980; Vago et al. 1997) whilst light-calcification is dominated by infilling of pores, resulting in a thickening of the skeleton and is more energetically costly (Barnes 1970; Gattuso et al. 2015; Wooldridge 2013). A disruption or imbalance in these calcification stages may contribute to structural changes observed in coral skeletons under sub-optimal conditions. Light-calcification is thought to be facilitated by the additional energy derived from zooxanthellae (Gattuso et al. 2015; Neder et al. 2022) and as ambient seawater at night is naturally more acidic and possesses lower oxygen content than during the day (Albright et al. 2013; Gobler and Baumann 2016; Shashar et al. 1993), the dark-calcification mechanisms may be better suited to cope with perceived stressors. A reduction in light-calcification compared to dark-calcification may lead to a more porous and thinner skeletal phenotype, as observed in *P. acuta*, due to reduced infilling whilst maintaining a constant linear extension rate.

Pocillopora acuta was the only species of the three studied that was found at all sites at the time of sampling. *Pocillopora sp.* are known to be a pioneering taxon (Fabricius 2005; Uthicke et al. 2010) and exhibit tolerance for elevated nutrient levels which may contribute to its ability to persist in the mangrove environment (Muller-Parker et al. 1994; Stambler et al. 1991). *Pocillopora acuta's* reproductive method involving brooding of larvae (Fiesinger et al. 2023) may facilitate recruitment from resident stress resilient corals and contribute to its wide distribution at Low Isles (Ayre and Hughes 2000; Fiesinger et al. 2023). Further, asexual reproduction such as via fragmentation may also facilitate local recruitment from amongst the mangroves (Highsmith 1982; Lord et al. 2023).

In contrast, *M.* cf. *digitata* retained a similar skeletal structure at sites both within and outside the mangrove system. As *Montipora sp.* are known to be highly heterotrophic (Hughes and Grottoli 2013), this finding may suggest species more reliant on heterotrophy may not be as greatly impacted by sub-optimal conditions (Marshall and Baird 2000; Price et al. 2021). We found *M.* cf. *digitata* possessed a significantly lower density of corallites inside the mangroves and these were associated with larger calyxes. As the production of larger calyxes and, by extension, polyps is associated with increased heterotrophic feeding (Conti-Jerpe et al. 2020; Houlbreque and Ferrier-Pages 2009), this result supports the suggestion that increased feeding may counterbalance the energetic cost of biomineralisation under stressful conditions (Camp et al. 2019; Houlbreque et al. 2015; Tanvet

et al. 2022). Feeding effort and heterotrophic capacity may influence the ability of different coral species to utilise the available organic matter at mangroves for skeletal formation, where more heterotrophic species may be more capable of using these resources to produce skeletons structurally equivalent to those observed under normal conditions (Granek et al. 2009; Perry 2007; Tanvet et al. 2022).

Acropora cf. *millepora*, although previously observed at Woody Island (Camp et al. 2019), was not found in the mangroves at the time of sampling, potentially due to *Acropora sp.* sensitivity to stress conditions (Camp et al. 2016; Hughes et al. 2020; Johnson et al. 2021; Manullang et al. 2023). *Acropora* cf. *millepora* skeletons were more porous and thinner at the Low Isles reef compared to Opal Reef. The sensitivity of *A.* cf. *millepora* skeletons to mangrove stressors is evidenced from previous studies at the Low Isles, Woody Island mangroves, which found significant reductions in calcification rates of *A.* cf. *millepora* from the mangroves compared to the adjacent reef as well as increased respiration rates in the mangroves (Camp et al. 2019). Interestingly, we found the skeletons of *A.* cf. *millepora* 300 m away from the mangroves at the Inner Adjacent Reef site had a thicker, less porous skeleton than those 1 km away at the Outer Adjacent Reef, potentially due to the influence of tidal flow which enters the Low Isles reef flat near the Inner Adjacent Reef site, replenishing the area with non-mangrove associated waters and potentially lessening the effect of stressors (Schueth and Frank 2008). Observation that the thinnest skeletal structures for *A.* cf. *millepora* occurred at the Outer Adjacent Reef site contradicts suggestions that thinner and more porous skeletons at mangroves are the result of reduced wave energy (Scucchia et al. 2023). This is supported by foraminifera analysis which recorded high wave energy associated foraminifera namely, *Baculogypsina sp.* and *Calcarina sp.* (Lobegeier 2002), were found in abundance at Opal Reef but not at the Woody Island and Low Isles reef sites assessed (Chadda-Harmer et al. 2025).

Interspecies comparison found that skeletal surface area to volume ratios significantly differed between *P. acuta* and both *A.* cf. *millepora* and *M.* cf. *digitata*. *Acropora millepora* and *M. digitata* are perforate corals and share a similar skeletal architecture (Yost et al. 2013) whereas *P. acuta* is an imperforate coral (Huffmyer et al. 2020) which may explain the differences observed. The interconnected tissues penetrating skeletons in perforate corals has been suggested to enable coral polyps to cope better under environmental stress (Yost et al. 2013) but like the findings of Comeau et al. (2014), we did not observe a clear perforate advantage in skeletal formation.

Implications and future research

This study is the first multi-species assessment of the structure of coral skeletons in mangrove environments and provides insights on the skeletal integrity and potential coping mechanisms of corals within these systems. Structural analysis supports the hypothesis that for some species, e.g., *M.* cf. *digitata*, heterotrophy is a mechanism that may support coral survival within the sub-optimal conditions influenced by the mangrove forest. As particulate organic matter availability at reefs is projected to decrease under climate change (Kealoha et al. 2019), mangroves may provide an increasingly important nutrient resource and benefit nearby corals that grow at a distance far enough not to be impacted by mangrove stressors (Carlson et al. 2021). Considering mangroves as a model for future ocean conditions, results of the present study warn of the formation of weaker coral skeletons with increasing climate change associated stress. Species-specific responses to environmental stress suggest clear winners and losers, with a possible loss of diversity and altered coral community structure under future ocean conditions which threatens the structural complexity of coral reef habitats and the ecosystem they support (Agostini et al. 2021; Marshall and Baird 2000).

Coupling research on structural changes with investigation of other measures indicative of the inherent strength of skeletal material, such as biomineral hardness using nanoindentation (Fantazzini et al. 2015; Scucchia et al. 2023), will also be useful in determining the extent to which environmental stress impacts coral skeletons. Further, combining structural analysis with more commonly used metrics such as calcification rate and bulk density measurements will enable greater comparison across studies and increase our understanding of how changes in skeletal formation occur.

As natural systems are highly variable, future studies investigating the effect of distance from mangroves on corals are encouraged to utilise multiple replicate sites of the same distance to account for confounding factors such as tidal patterns and geomorphological settings. To better constrain the factors impacting corals in these environments it is encouraged that a suite of physiochemical data (e.g., pH, temperature, oxygen, aragonite saturation state, turbidity, light, and water organic carbon content) are collected at all sites corals are sampled from as well as hydrodynamic parameters. Future research on the skeletal integrity of mangrove associated corals will be important to better ascertain the potential of these sites to support coral growth under stress and delineate the factors most strongly contributing to skeletal changes in corals from these environments and under future ocean conditions.

Acknowledgements We would like to acknowledge the Traditional Owners of the Sea Country and land upon which this research was

conducted, the Kuku Yulanji and Yirrganydgi peoples of the Great Barrier Reef, and the Gadigal peoples of the Eora Nation on which the University of Sydney stands. We acknowledge the technical and scientific assistance of Sydney Microscopy & Microanalysis, the University of Sydney node of Microscopy Australia. We would also like to thank Wavelength Reef Cruises for their assistance with mangrove and reef site access, Christine Roper and Chiara Duijser for assistance with sample collection, Ann Huajuan Ling for assistance in conducting loss on ignition analysis, Liav Meoded Stern for help with corallite photomicroscopy, Augustine Crosbie for assistance with coral ID and Neeru Chadda for manuscript feedback. We also thank the reviewers and editor for their insightful comments and suggestions. This research was supported by the Australian Research Council (grant number DE220100555, SAF; DP220101125, MB), a Westpac Research Fellowship from the Westpac Scholars Trust and a Horizon Fellowship from the University of Sydney.

Author contribution D.C-H wrote the main manuscript text, prepared figures and conducted formal analysis. D.C-H, S.A.F, M.F and G.B-S conducted investigation. S.A.F, M.B and E.F.C provided resources. S.A.F provided supervision. All authors reviewed the manuscript.

Funding Open Access funding enabled and organized by CAUL and its Member Institutions.

Data availability Data will be made available upon request.

References

Agostini S, Houlbrèque F, Biscéré T, Harvey BP, Heitzman JM, Takimoto R, Yamazaki W, Milazzo M, Rodolfo-Metalpa R (2021) Greater mitochondrial energy production provides resistance to ocean acidification in "Winning" Hermatypic Corals. Front Marine Sci. https://doi.org/10.3389/fmars.2020.600836

Albright R, Langdon C, Anthony KRN (2013) Dynamics of seawater carbonate chemistry, production, and calcification of a coral reef flat, central Great Barrier Reef. Biogeosciences 10:6747–6758. https://doi.org/10.5194/bg-10-6747-2013

Al-Horani FA, Tambutté É, Allemand D (2007) Dark calcification and the daily rhythm of calcification in the scleractinian coral, *Galaxea fascicularis*. Coral Reefs 26(3):531–538. https://doi.org/10.1007/s00338-007-0250-x

Allison N, Ross P, Brasier A, Cieminska N, Lopez Martin N, Cole C, Hintz C, Hintz K, Finch A (2022) Effects of seawater pCO2 on the skeletal morphology of massive *Porites* spp. corals. Mar Biol. https://doi.org/10.1007/s00227-022-04060-9

Altieri AH, Nelson HR, Gedan KB (2019) The significance of ocean deoxygenation for tropical ecosystems – corals, seagrasses and mangroves. In: D. Laffoley & J. M. Baxter (Eds.), *Ocean deoxygenation: Everyone's problem - Causes, impacts, consequences and solutions* (pp. 401–432). IUCN. https://doi.org/10.2305/IUCN.CH.2019.13.en

Ayre DJ, Hughes TP (2000) Genotypic diversity and gene flow in brooding and spawning corals along the Great Barrier Reef, Australia. Evolution 54(5):1590–1605. https://doi.org/10.1111/j.0014-3820.2000.tb00704.x

Barnes DJ (1970) Coral skeletons: an explanation of their growth and structure. Science 170(3964):1305–1308

Barnes DJ, Crossland CJ (1980) Diurnal and seasonal variations in the growth of a staghorn coral measured by time-lapse photography. Limnol Oceanogr 25(6):1113–1117. https://doi.org/10.4319/lo.1980.25.6.1113

Bartels N, Dilernia NJ, Howlett L, Camp EF (2023) Stress event for "super corals" in Great Barrier Reef mangrove lagoon. Mar Biodivers 53(5):64. https://doi.org/10.1007/s12526-023-01374-9

Bates D, Mächler M, Bolker B, Walker S (2015) Fitting linear mixed-effects models using lme4. J Stat Softw 67(1):1–48. https://doi.org/10.18637/jss.v067.i01

Burt JA, Camp EF, Enochs IC, Johansen JL, Morgan KM, Riegl B, Hoey AS (2020) Insights from extreme coral reefs in a changing world. Coral Reefs 39(3):495–507. https://doi.org/10.1007/s00338-020-01966-y

Byrne M, Fitzer S (2019) The impact of environmental acidification on the microstructure and mechanical integrity of marine invertebrate skeletons. Conserv Physiol 7(1):coz062. https://doi.org/10.1093/conphys/coz062

Camp EF, Suggett DJ, Gendron G, Jompa J, Manfrino C, Smith DJ (2016) Mangrove and seagrass beds provide different biogeochemical services for corals threatened by climate change. Front Marine Sci. https://doi.org/10.3389/fmars.2016.00052

Camp EF, Nitschke MR, Rodolfo-Metalpa R, Houlbreque F, Gardner SG, Smith DJ, Zampighi M, Suggett DJ (2017) Reef-building corals thrive within hot-acidified and deoxygenated waters. Sci Rep 7(1):2434. https://doi.org/10.1038/s41598-017-02383-y

Camp EF, Schoepf V, Mumby PJ, Hardtke LA, Rodolfo-Metalpa R, Smith DJ, Suggett DJ (2018) The future of coral reefs subject to rapid climate change: lessons from natural extreme environments. Front Marine Sci. https://doi.org/10.3389/fmars.2018.00004

Camp EF, Edmondson J, Doheny A, Rumney J, Grima AJ, Huete A, Suggett DJ (2019) Mangrove lagoons of the Great Barrier Reef support coral populations persisting under extreme environmental conditions. Mar Ecol Prog Ser 625:1–14. https://doi.org/10.3354/meps13073

Carlson RR, Evans LJ, Foo SA, Grady BW, Li J, Seeley M, Xu Y, Asner GP (2021) Synergistic benefits of conserving land-sea ecosystems. Glob Ecol Conserv 28:e01684. https://doi.org/10.1016/j.gecco.2021.e01684

Caroselli E, Prada F, Pasquini L, Marzano FN, Zaccanti F, Falini G, Levy O, Dubinsky Z, Goffredo S (2011) Environmental implications of skeletal micro-density and porosity variation in two scleractinian corals. Zoology (Jena) 114(5):255–264. https://doi.org/10.1016/j.zool.2011.04.003

Chadda-Harmer D, Byrne M, Reymond CE, Fellowes TE, Camp EF, Foo SA (2025) Benthic foraminifera as bioindicators of coral condition near mangrove environments. Mar Environ Res 209:107159. https://doi.org/10.1016/j.marenvres.2025.107159

Chamberlain JA (1978) Mechanical properties of coral skeleton: compressive strength and its adaptive significance. Paleobiology 4(4):419–435. https://doi.org/10.1017/S0094837300006163

Comeau S, Edmunds PJ, Spindel NB, Carpenter RC (2014) Fast coral reef calcifiers are more sensitive to ocean acidification in

short-term laboratory incubations. Limnol Oceanogr 59(3):1081–1091. https://doi.org/10.4319/lo.2014.59.3.1081

Comeau S, Cornwall CE, Shlesinger T, Hoogenboom M, Mana R, McCulloch MT, Rodolfo-Metalpa R (2022) pH variability at volcanic CO(2) seeps regulates coral calcifying fluid chemistry. Glob Chang Biol 28(8):2751–2763. https://doi.org/10.1111/gcb.16093

Conti-Jerpe IE, Thompson PD, Wong CWM, Oliveira NL, Duprey NN, Moynihan MA, Baker DM (2020) Trophic strategy and bleaching resistance in reef-building corals. Sci Adv 6(15):eaaz5443–eaaz5443. https://doi.org/10.1126/sciadv.aaz5443

Dávalos-Dehullu E, Hernández-Arana H, Carricart-Ganivet JP (2008) On the causes of density banding in skeletons of corals of the genus *Montastraea*. J Exp Mar Biol Ecol 365(2):142–147. https://doi.org/10.1016/j.jembe.2008.08.008

Dean WE (1974) Determination of carbonate and organic matter in calcareous sediments and sedimentary rocks by loss on ignition: comparison with other methods. J Sediment Res. https://doi.org/10.1306/74D729D2-2B21-11D7-8648000102C1865D

Decarlo T (2017) Deriving coral skeletal density from computed tomography (CT): effects of scan and reconstruction settings. Matters Select. https://doi.org/10.19185/matters.201706000005

eReefs (2019) 4km eReefs Biogeochemical model (v3.1). https://ereefs.aims.gov.au/. https://ereefs.aims.gov.au/

Fabricius KE (2005) Effects of terrestrial runoff on the ecology of corals and coral reefs: review and synthesis. Mar Pollut Bull 50(2):125–146. https://doi.org/10.1016/j.marpolbul.2004.11.028

Fairhall AW (1973) Accumulation of fossil CO2 in the atmosphere and the sea. Nature 245(5419):20–23. https://doi.org/10.1038/245020a0

Fantazzini P, Mengoli S, Pasquini L, Bortolotti V, Brizi L, Mariani M, Di Giosia M, Fermani S, Capaccioni B, Caroselli E, Prada F, Zaccanti F, Levy O, Dubinsky Z, Kaandorp JA, Konglerd P, Hammel JU, Dauphin Y, Cuif JP, Weaver JC, Fabricius KE, Wagermaier W, Fratzl P, Falini G, Goffredo S (2015) Gains and losses of coral skeletal porosity changes with Ocean acidification acclimation. Nat Commun 6:7785. https://doi.org/10.1038/ncomms8785

Fiesinger A, Held C, Melzner F, Putchim L, Reusch TBH, Schmidt AL, Wall M (2023) Population genetic differentiation of the ubiquitous brooding coral *Pocillopora acuta* along Phuket Island reefs in the Andaman Sea, Thailand. BMC Ecol Evol 23:42. https://doi.org/10.1186/s12862-023-02153-7

Fordyce AJ, Knuefing L, Ainsworth TD, Beeching L, Turner M, Leggat W, Pracheil B (2020) Understanding decay in marine calcifiers: Micro-CT analysis of skeletal structures provides insight into the impacts of a changing climate in marine ecosystems. Methods Ecol Evol 11(9):1021–1041. https://doi.org/10.1111/2041-210x.13439

Gattuso J-P, Allemand D, Frankignoulle M (2015) Photosynthesis and calcification at cellular, organismal and community levels in coral reefs: a review on interactions and control by carbonate chemistry. Am Zool 39(1):160–183. https://doi.org/10.1093/icb/39.1.160

Gladfeiter EH (1982) Skeletal development in *Acropora cervicornis*: I. Patterns of calcium carbonate accretion in the axial corallite. Coral Reefs 1(1):45–51. https://doi.org/10.1007/BF00286539

Gobler CJ, Baumann H (2016) Hypoxia and acidification in ocean ecosystems: coupled dynamics and effects on marine life. Biol Lett 12(5):20150976. https://doi.org/10.1098/rsbl.2015.0976

Granek EF, Compton JE, Phillips DL (2009) Mangrove-exported nutrient incorporation by sessile coral reef invertebrates. Ecosystems 12(3):462–472. https://doi.org/10.1007/s10021-009-9235-7

Haydon TD, Seymour JR, Raina JB, Edmondson J, Siboni N, Matthews JL, Camp EF, Suggett DJ (2021) Rapid shifts in bacterial communities and homogeneity of Symbiodiniaceae in colonies of Pocillopora acuta transplanted between reef and mangrove environments. Front Microbiol 12:756091. https://doi.org/10.3389/fmicb.2021.756091

Heiri O, Lotter AF, Lemcke G (2001) Loss on ignition as a method for estimating organic and carbonate content in sediments: reproducibility and comparability of results. J Paleolimnol 25(1):101–110. https://doi.org/10.1023/A:1008119611481

Highsmith RC (1982) Reproduction by fragmentation in corals. Mar Ecol Prog Ser 7:207–226

Hoegh-Guldberg O, Pendleton L, Kaup A (2019) People and the changing nature of coral reefs. Reg Stud Mar Sci 30:100699. https://doi.org/10.1016/j.rsma.2019.100699

Horvath KM, Castillo KD, Armstrong P, Westfield IT, Courtney T, Ries JB (2016) Next-century ocean acidification and warming both reduce calcification rate, but only acidification alters skeletal morphology of reef-building coral *Siderastrea siderea*. Sci Rep 6:29613. https://doi.org/10.1038/srep29613

Houlbreque F, Ferrier-Pages C (2009) Heterotrophy in tropical scleractinian corals. Biol Rev 84(1):1–17. https://doi.org/10.1111/j.1469-185X.2008.00058.x

Houlbreque F, Reynaud S, Godinot C, Oberhansli F, Rodolfo-Metalpa R, Ferrier-Pages C (2015) Ocean acidification reduces feeding rates in the scleractinian coral *Stylophora pistillata*. Limnol Oceanogr 60:89–99. https://doi.org/10.1002/lno.10003

Howells EJ, Dunshea G, McParland D, Vaughan GO, Heron SF, Pratchett MS, Burt JA, Bauman AG (2018) Species-specific coral calcification responses to the extreme environment of the southern Persian Gulf. Front Mar Sci 5:56. https://doi.org/10.3389/fmars.2018.00056

Howlett L, Camp EF, Edmondson J, Henderson N, Suggett DJ (2021) Coral growth, survivorship and return-on- effort within nurseries at high-value sites on the Great Barrier Reef. PLoS ONE 16(1):e0244961. https://doi.org/10.1371/journal.pone.0244961

Huffmyer AS, Matsuda SB, Eggers AR, Lemus JD, Gates RD (2020) Evaluation of laser scanning confocal microscopy as a method for characterizing reef-building coral tissue thickness and Symbiodiniaceae fluorescence. J Experiment Biol 223:220335. https://doi.org/10.1242/jeb.220335

Hughes AD, Grottoli AG (2013) Heterotrophic Compensation: A Possible Mechanism for Resilience of Coral Reefs to Global Warming or a Sign of Prolonged Stress? PLoS One, 8(11):e81172. https://doi.org/10.1371/journal.pone.0081172

Hughes TP, Barnes ML, Bellwood DR, Cinner JE, Cumming GS, Jackson JBC, Kleypas J, van de Leemput IA, Lough JM, Morrison TH, Palumbi SR, van Nes EH, Scheffer M (2017) Coral reefs in the Anthropocene. Nature 546(7656):82–90. https://doi.org/10.1038/Nature22901

Hughes DJ, Alderdice R, Cooney C, Kühl M, Pernice M, Voolstra CR, Suggett DJ (2020) Coral reef survival under accelerating ocean deoxygenation. Nat Clim Chang 10(4):296–307. https://doi.org/10.1038/s41558-020-0737-9

IPCC (2022) Climate Change 2022: Impacts, adaptation, and vulnerability. contribution of working Group II to the sixth assessment report of the intergovernmental panel on climate change [H.-O. Pörtner, D.C. Roberts, M. Tignor, E.S. Poloczanska, K. Mintenbeck, A. Alegría, M. Craig, S. Langsdorf, S. Löschke, V. Möller, A. Okem, B. Rama (eds.)]. Cambridge University Press. Cambridge University Press, Cambridge, UK and New York, NY, USA, 3056 pp., https://doi.org/10.1017/9781009325844.

Johnson MD, Swaminathan SD, Nixon EN, Paul VJ, Altieri AH (2021) Differential susceptibility of reef-building corals to deoxygenation reveals remarkable hypoxia tolerance. Sci Rep 11(1):23168. https://doi.org/10.1038/s41598-021-01078-9

Kealoha AK, Shamberger KEF, Reid EC, Davis KA, Lentz SJ, Brainard RE, Oliver TA, Rappé MS, Roark EB, Rii YM (2019) Heterotrophy of oceanic particulate organic matter elevates net ecosystem

calcification. Geophys Res Lett 46(16):9851–9860. https://doi.org/10.1029/2019gl083726
Kramer N, Guan J, Chen S, Wangpraseurt D, Loya Y (2022) Morpho-functional traits of the coral *Stylophora pistillata* enhance light capture for photosynthesis at mesophotic depths. Commun Biol 5(1):861. https://doi.org/10.1038/s42003-022-03829-4
Kuznetsova A, Brockhoff PB, Christensen RHB (2017) LmerTest package: tests in linear mixed effects models. J Stat Softw 82(13):1–26. https://doi.org/10.18637/jss.v082.i13
Lenth R (2025) Emmeans: Estimated marginal means, aka least-squares means. R package version 1.11.1–00001. https://rvlenth.github.io/emmeans/.
Lobegeier MK (2002) Benthic foraminifera of the family calcarinidae from Green Island Reef, Great Barrier Reef Province. J Foraminifer Res 32(3):201–216. https://doi.org/10.2113/32.3.201
Lord KS, Lesneski KC, Buston PM, Davies SW, D'Aloia CC, Finnerty JR (2023) Rampant asexual reproduction and limited dispersal in a mangrove population of the coral *Porites divaricata*. Proc Biol Sci 290(2002):20231070
Love CR, Speare KE, Fox MD, Radice VZ, McMahon KW, Hofmann GE, Valentine DL, Strader ME (2025) Heterotrophy of particulate organic matter subsidies contributes to divergent bleaching responses in tropical *Scleractinian* corals. Limnol Oceanogr. https://doi.org/10.1002/lno.70085
Lüdecke D, Ben-Shachar MS, Patil I, Waggoner P, Makowski D (2021) Performance: an R package for assessment, comparison and testing of statistical models. J Open Source Softw 6(60):3139. https://doi.org/10.21105/joss.03139
Manullang C, Singh T, Sakai K, Miyagi A, Iwasaki A, Nojiri Y, Iguchi A (2023) Separate and combined effects of elevated pCO2 and temperature on the branching reef corals Acropora digitifera and Montipora digitata. Mar Environ Res 188:106030. https://doi.org/10.1016/j.marenvres.2023.106030
Marshall PA, Baird AH (2000) Bleaching of corals on the Great Barrier Reef: differential susceptibilities among taxa. Coral Reefs 19:155–163. https://doi.org/10.1007/s003380000086
Muller-Parker G, McCloskey LR, Hoegh-Guldberg O, McAuley PJ (1994) Effect of ammonium enrichment on animal and algal biomass of the coral pocillopora damicornis. Pacific Science, 48(3).
Neder M, Saar R, Malik A, Antler G, Mass T (2022) New insights on the diurnal mechanism of calcification in the stony coral, Stylophora pistillata. Front Mar Sci. https://doi.org/10.3389/fmars.2021.745171
Otsu N (1979) A threshold selection method from gray-level histograms. IEEE Trans Syst Man Cybern 9(1):62–66. https://doi.org/10.1109/TSMC.1979.4310076
Perry C (2007) Tropical coastal environments: coral reefs and mangroves. In: Perry C, Taylor K (eds) Environmental Sedimentology. Blackwell Publishing, pp 302–350. 9781405115155.
Poloczanska ES, Burrows MT, Brown CJ, García Molinos J, Halpern BS, Hoegh-Guldberg O, Kappel CV, Moore PJ, Richardson AJ, Schoeman DS, Sydeman WJ (2016) Responses of marine organisms to climate change across oceans. Front Marine Sci. https://doi.org/10.3389/fmars.2016.00062
Prada F, Brizi L, Franzellitti S, Mengoli S, Fermani S, Polishchuk I, Baraldi N, Ricci F, Palazzo Q, Caroselli E, Pokroy B, Giorgini L, Dubinsky Z, Fantazzini P, Falini G, Goffredo S, Fabricius KE (2021) Coral micro- and macro-morphological skeletal properties in response to life-long acclimatization at CO(2) vents in Papua New Guinea. Sci Rep 11(1):19927. https://doi.org/10.1038/s41598-021-98976-9
Price JT, McLachlan RH, Jury CP, Toonen RJ, Grottoli AG (2021) Isotopic approaches to estimating the contribution of heterotrophic sources to Hawaiian corals. Lim Ocean, 66: 2393–2407. https://doi.org/10.1002/lno.11760
R Core Team (2022). R: A language and environment for statistical computing. In: (Version 4.2.2) https://www.R-project.org/
Roche RC, Abel RL, Johnson KG, Perry CT (2011) Spatial variation in porosity and skeletal element characteristics in apical tips of the branching coral *Acropora pulchra* (Brook 1891). Coral Reefs 30(1):195–201. https://doi.org/10.1007/s00338-010-0679-1
Schneider CA, Rasband WS, Eliceiri KW (2012) NIH image to ImageJ: 25 years of image analysis. Nat Methods 9(7):671–675. https://doi.org/10.1038/nmeth.2089
Schoepf V, Baumann JH, Barshis DJ, Browne NK, Camp EF, Comeau S, Cornwall CE, Guzman HM, Riegl B, Rodolfo-Metalpa R, Sommer B (2023) Corals at the edge of environmental limits: a new conceptual framework to re-define marginal and extreme coral communities. Sci Total Environ 884:163688. https://doi.org/10.1016/j.scitotenv.2023.163688
Schueth JD, Frank TD (2008) Reef foraminifera as bioindicators of coral reef health: low Isles Reef, Northern Great Barrier Reef. Australia the J Foraminiferal Res 38(1):11–22. https://doi.org/10.2113/gsjfr.38.1.11
Scucchia F, Zaslansky P, Boote C, Doheny A, Mass T, Camp EF (2023) The role and risks of selective adaptation in extreme coral habitats. Nat Commun 14:4475. https://doi.org/10.1038/s41467-023-39651-7
Shashar N, Cohen Y, Loya Y (1993) Extreme diel fluctuations of oxygen in diffusive boundary layers surrounding stony corals. Biol Bull 185(3):455–461. https://doi.org/10.2307/1542485
Silverman BW (1986) Density estimation for statistics and data analysis. Monographs on Statistics and Applied Probability. Chapman and Hall, London. 0412246201.
Stambler, N., Popper, N., Dubinsky, Z., & Stimson, J. (1991). Effects of Nutrient Enrichment and Water Motion on the Coral Pocillopora damicornis. *Pacific Science*, *45*(3).
Tambutte E, Venn AA, Holcomb M, Segonds N, Techer N, Zoccola D, Allemand D, Tambutte S (2015) Morphological plasticity of the coral skeleton under CO2-driven seawater acidification. Nat Commun 6:7368. https://doi.org/10.1038/ncomms8368
Tanvet C, Camp E, Sutton J, Houlbreque F, Thouzeau G, Rodolfo-Metalpa R (2022) Corals adapted to extreme and fluctuating seawater pH increase calcification rates and have unique symbiont communities. Ecol Evol. https://doi.org/10.22541/au.166903223.33049825/v1
Uthicke S, Thompson A, Schaffelke B (2010) Effectiveness of benthic foraminiferal and coral assemblages as water quality indicators on inshore reefs of the Great Barrier Reef, Australia. Coral Reefs 29:209–225. https://doi.org/10.1007/s00338-009-0574-9
Uthicke S, Furnas M, Lonborg C (2014) Coral reefs on the edge? Carbon chemistry on inshore reefs of the Great Barrier Reef. PLoS ONE 9(10):e109092. https://doi.org/10.1371/journal.pone.0109092
Vago R, Gill E, Collingwood JC (1997) Laser measurements of coral growth. Nature 386(6620):30–31. https://doi.org/10.1038/386030a0
Wickham H (2016) ggplot2: Elegant graphics for data analysis. Springer, New York. https://doi.org/10.1007/978-0-387-98141-3
Wickham H, Averick M, Bryan J, Chang W, McGowan L, François R, Grolemund G, Hayes A, Henry L, Hester J, Kuhn M, Pedersen T, Miller E, Bache S, Müller K, Ooms J, Robinson D, Seidel D, Spinu V, Takahashi K, Vaughan D, Wilke C, Woo K, Yutani H (2019) Welcome to the tidyverse. J Open Source Softw 4(43):1686. https://doi.org/10.21105/joss.01686
Wooldridge S (2013) A new conceptual model of coral biomineralisation: hypoxia as the physiological driver of skeletal extension. Biogeosciences 10(5):2867–2884. https://doi.org/10.5194/bg-10-2867-2013
Yates KK, Rogers CS, Herlan JJ, Brooks GR, Smiley NA, Larson RA (2014) Diverse coral communities in mangrove habitats suggest a

novel refuge from climate change. Biogeosciences 11(16):4321–4337. https://doi.org/10.5194/bg-11-4321-2014

Yost DM, Wang LH, Fan TY, Chen CS, Lee RW, Sogin E, Gates RD (2013) Diversity in skeletal architecture influences biological heterogeneity and *Symbiodinium* habitat in corals. Zoology (Jena) 116(5):262–269. https://doi.org/10.1016/j.zool.2013.06.001